Catalysis Today 271 (2016) 102–113

Contents lists available at ScienceDirect

Catalysis Today

journal homepage: www.elsevier.com/locate/cattod

Sulfur elimination by oxidative desulfurization with titanium-modified SBA-16

Lorena P. Rivoira, Verónica A. Vallés, Brenda C. Ledesma, María V. Ponte, María L. Martínez, Oscar A. Anunziata, Andrea R. Beltramone*

Centro de Investigación en Nanociencia y Nanotecnología (NANOTEC), Facultad Regional Córdoba, Universidad Tecnológica Nacional, Maestro López y Cruz Roja Argentina, 5016 Córdoba, Argentina

ARTICLE INFO

Article history:
Received 31 March 2015
Received in revised form 16 July 2015
Accepted 21 July 2015
Available online 28 September 2015

Keywords:
Ti-containing SBA-16
TiO_2
Ti incorporation method
ODS
Reaction kinetics

ABSTRACT

TiO_2-modified mesoporous SBA-16 and titanium-substituted mesoporous SBA-16 were developed and tested in the oxidative desulfurization (ODS) of dibenzothiophene prevailing in liquid fuel. Pure TiO_2 was used as reference. The titania-based catalysts were characterized by chemical analysis, XRD, EDX and TEM. The titanium state as tetrahedral (in Ti-SBA-16 sample) or octahedral (in TiO_2/SBA-16 sample) coordination surrounding in the silicate matrix was determined by XPS, UV–vis DRS, FTIR, Raman and XANES. We assessed the impact exerted on performance of different reaction variables, including (nature and amount of the active catalytic species, phase system, molar ratio of oxidant H_2O_2 and DBT, reaction temperature, nature of the substrate and reuse of catalysts). In addition, we carried out a kinetic study and the activation energy was determined. We achieved 90% of S removal from a 0.2 wt.% dibenzothiophene solution at 60 °C in less than 1 h of reaction. The best catalytic results are obtained with high exposed surface of nanometric TiO_2 species of TiO_2/SBA-16 sample. The activated catalyst is very active in ODS reaction and can be reused four times with no loss in activity.

1. Introduction

Over the past, oxidative desulfurization (ODS) has drawn considerable interest as a new alternative method for deep sulfur elimination from light oils. This can be attributed to its attractive properties, including lower temperature and pressure conditions and lower operating cost [1–10] than conventional hydrodesulfurization (HDS) process. Oxidation of organosulfur compounds results in the formation of sulfoxides/sulfones, highly polar and hence easily removed by both extraction into polar solvents or by adsorption. Due to their low reactivity, dibenzothiophene derivatives (DBTs) are the most refractory species to be eliminated from oils [11–15]. Hence, the ODS process through which DBTs are converted to their corresponding sulfones involves great interest at present [11–23].

Hydroprocessing reactions via competitive adsorption can be strongly inhibited by the sulfur and nitrogen compounds found in synthetic feedstock and heavy petroleum fractions. Even at low concentrations, these species, limit the catalytic activity found, and thus require higher pressures and temperatures to obtain the desired conversions. Catalytic oxidation of organic sulfur compounds has been reported to use molecular sieves as catalysts under mild conditions. Oxidative desulfurization (ODS) process occurs in a three-phase (L–L–S) system consisted of two liquid phases, model diesel and extraction solvent, and a solid catalyst. Usually comprising two simultaneous extraction and oxidation steps [11,12]. When these phases are mixed, DBTs present in the diesel phase are partially extracted to the solvent phase, where oxidant reagent is predominantly present, and the oxidation reaction takes place therein producing the corresponding sulfone, the sulfur compound, the solid catalyst and the oxidizing agent are in the polar phase and yield the sulfone derivatives of the corresponding sulfur compound. This facilitates the separation of the sulfone from the diesel.

This process is characterized by two major aspects: absence of hydrogen, and in some cases the reactivity trend order of the S-molecules proceeds inversely than in the HDS process when peracids such as formic or acetic acid are used as oxidizing agents [11,14]. The organic sulfides could be oxidized with hydrogen peroxide as an oxidizing agent [24]. The oxidation of DBTs with organic hydroperoxides or H_2O_2 was studied over various catalytic heterogeneous systems, such as supported oxide metals [14,25] or titanium silicalites [26,27]. Vanadosilicates were used as catalysts for the desulfurization of light oil [28–30]. The oxidation of (DBTs) was also performed using WO_x/ZrO_2 catalyst [31],

* Corresponding author.
E-mail address: abeltramone@scdt.frc.utn.edu.ar (A.R. Beltramone).

http://dx.doi.org/10.1016/j.cattod.2015.07.055
0920-5861/

supported Pd, Cr_2O_3, unsupported manganese oxides and a commercial Co-Mo/Al_2O_3 with hydrogen peroxide as oxidant [32].

In general, when tetravalent cations like Ti^{4+}, Zr^{4+}, V^{4+}, Sn^{4+}, etc. are incorporated to the framework of SBA-15, the electroneutrality is maintained but some redox properties are incorporated to the support surface [33]. Rayo et al. [34] studied the effect of the incorporation of Al, Ti, and Zr on SBA-15. They found that beyond 20 wt.% of heteroatom, the segregation of metal oxides on the surface becomes significant and there is an important decrease in the surface area and pore volume of the support, which negatively affects the dispersion of the active phases leading to a decrease in catalytic activity. The addition of 5–10 wt.% Ti to the catalyst caused greater increases in activity than those obtained with Zr.

In view of recent studies, Ti-containing molecular sieves show good activity in the oxidation of different S-bearing compounds [35,36]. Titanium silicalite (TS-1) is used as a catalyst in the selective oxidation of thiophene at 60 °C; 90% thiophene conversion was achieved in 1 h of reaction. Here, framework titanium species was found to be the active site for thiophene oxidation.

Typical catalytic supports, such as alumina, titania and silica, exhibit low ODS activity of DBTs; thus differences in their activity cannot be correlated with surface area [25,37–39]. New large surface area Ti-containing materials such as mesoporous Ti-modified SBA-15 and titanium oxide nanotubes could prove alternatives catalysts for the ODS process [40].

Cedeño-Caero et al. [40], using Ti-nanotubes attribute the ODS activity to the TiO_2 surface exposed. Lorençon et al. [41] also investigated the catalytic activity of titanate nanotubes in the oxidation of DBT by using hydrogen peroxide. Chica et al. [26] reported the activity and stability in ODS of mesoporous Ti-containing materials, using organic peroxides as oxidants over a fixed-bed reactor. They observed that Ti-MCM-41 catalyst was more active and stable than Ti-beta and MoO_3/Al_2O_3 catalysts without Ti-leaching. The surface was modified by silylation to diminish the adsorption of the more polar sulfones that will strongly contribute to catalyst deactivation. Hulea et al. [24] and Corma et al. [42] studied the reaction of sulfides with hydrogen peroxide on TS-1 and Ti-beta and with tert-butyl hydroperoxide on Ti-beta and Ti-MCM-41, respectively, using various organic solvents. They found that Ti-MCM-41 was more active than TS-1. More recently, Ti-SBA-15 catalysts were reported to exhibit high activity in ODS [43] either in a batch or in a continuous fixed-bed reactor with TBHP as oxidant [44]. ODS trend was found to decrease in the order of DBT > 4-MDBT > 4,6-DMDBT > BT. Ti-SBA-15 materials, as opposed to Ti-MCM-41 catalysts, was proved to be hydrolytically stable toward aqueous H_2O_2 [45].

Shah et al. [46] showed the experimental results of oxidative desulfurization (ODS) for Ti-SBA-16 with different titanium content. Findings indicate that all catalysts were highly active in the ODS of dibenzothiophene and their catalytic activity was unaffected up to 10 wt.% loading; Yet, further increase in Ti contents (15 wt.%) showed a slight decrease in catalyst activity. They ascribed that to the presence of high Ti content, causing slight structure change.

However, insights into SBA-16 support are scarce or inexistent. Purely siliceous SBA-16 (Im3m) was selected due to its high surface area and high thermal stability, but particularly, due to its attractive three-dimensional mesoporous structure. Comprising large spherical cavities arranged in a body-centered cubic array and connected through smaller mesoporous openings along (1 1 1) directions [47], that could favor the mass transfer kinetics compared with unidirectional pore system of other mesoporous.

We recently reported a good performance of this support in hydrotreating processes [48,49]. In this paper, we describe the preparation and characterization of new mesoporous catalytic materials based on Ti-containing SBA-16. We study here, the effect of the preparation method of titania-modified SBA-16 (characteristics of the active Ti and/or TiO_2 species) and the effect of the different operation conditions in ODS of DBT under mild conditions in order to find the best performance.

2. Experimental

2.1. Synthesis of the titanium-SBA-16 modified catalysts

Mesoporous silica materials with cubic Im3m structure Si-SBA-16 were synthesized according to the procedure described by the literature [50]. The molar composition of the mixture was: F127/TEOS/HCl/H_2O = 0.004/1/4/116. The incorporation of titanium species via the post-synthesis method to obtain TiO_2/SBA-16 was as follows: as-synthesized SBA-16 was dried in oven at 80 °C for 4 h. Then, 0.5 g of dried sample was dispersed in a solution containing 2 mL of titanium-tetrabutyl-orthotitanate (TTBT) and 5 mL of ethanol. The mixture was stirred at 60 °C for 2 h. The hybrid products were afterwards dried in a rotator evaporator in vacuum at 80 °C and calcined in air at 500 °C, with a heating rate of 5 °C/min for 4 h. Three TiO_2/SBA-16 samples were prepared with different content of TiO_2: 15, 20 and 26 wt.% denoted as TiO_2/SBA-16: samples A, B and C, respectively.

The incorporation of titanium as heteroatom in the SBA-16 mesoporous matrix was performed during the synthesis, following the method informed in our previous work [49]. We introduce here some modifications to the synthesis: pluronic F127 (EO106PO70EO106) was dissolved in a solution of distilled water and concentrated hydrochloric acid (37 wt.%). The solution was further stirred at 35 °C during 2 h, and TEOS was then added dropwise to the solution, stirring for another 15 min. Subsequently, tetraethyl-orthotitanate (TEOT) was dissolved in 10 mL of ethanol to avoid hydrolyzation and added slowly to the solution while stirring for another 24 h. The resulting suspension was transferred to the PP bottle and reposed under static conditions at 80 °C for 24 h. Ti-SBA-16 samples were prepared with different Si/Ti ratio (20, 15 and 10). The material obtained was denoted as Ti-SBA-16: samples D (Si/Ti = 20), E (Si/Ti = 15) and F (Si/Ti = 10).

Pure TiO_2 in anatase phase was prepared for comparison. In the synthesis procedure, soles of TiO_2 were prepared from a mixture of titanium tetraisopropoxide (TTIP), acetylacetonate (ACAC), de-ionized water (H_2O) and ethanol (EtOH) with a molar ratio of 1:1:3:20. The sol–gel stayed at room temperature during 24 h and then it was washed with de-ionized water and EtOH. Afterwards, the sample was dried at 90 °C during 24 h. To obtain anatase phase, two consecutive heat treatments were used: Inert post-treatment: N_2 (2 mL/min); 20–100 °C, 1 °C/min; 100 °C = 4 h; 100–400 °C, 2 °C/min; 400 °C = 10 h; 400–25 °C, −2 °C/min. Oxidative post-treatment: O_2 (5 mL/min); 20–100 °C, 1 °C/min; 100 °C = 4 h; 100–400 °C, 2 °C/min; 400 °C = 10 h; 400–25 °C, −2 °C/min. The anatase obtained had 95 m^2/g of specific surface area and 40–50 nm of mean crystal size. The material yielded was identified as TiO_2.

2.2. Characterization of the catalysts

XRD patterns were collected by using a continuous scan mode with a scan speed of 0.02° (2θ)/min in the Philips X'Pert PRO PANalytical diffractometer, operating with CuKα X-ray radiation (X-ray generator current and voltage set at 40 mA and 45 kV), using small divergence and scattering slits of 1/32 mm and a goniometer speed of 1.2° (2θ)/min. The scanning range was set between 0.5° and 5°.

The sample was crushed previously and placed in an aluminum sample holder. Elemental analysis was performed by inductively coupled plasma-atomic emission spectroscopy (VISTA-MPX) operated with high frequency emission power of 1.5 kW and plasma airflow of 12.0 L/min. The surface area was determined by the

BET method using a Micromeritics Chemisorb 2720 apparatus, equipped with a TCD detector, after degassing the samples with N_2 (25 mL/min) at 400 °C. Ultraviolet–visible diffuse reflectance spectroscopy (UV–vis DRS) was used to evaluate the relative distribution of octahedrally to tetrahedrally coordinated Ti species in the samples. The spectra were recorded with a Perkin Elmer Lamba 650 spectrophotometer equipped with a diffuse reflectance accessory. Raman spectrum was obtained from an InVia Reflex Raman microscope and spectrometer using a 532 nm diode laser excitation. X-ray photoelectron spectra (XPS) were obtained on a MicrotechMultilb 3000 spectrometer, equipped with a hemispherical electron analyzer and MgKα ($h\nu$ = 1253.6 eV) photon source. An estimated error of ±0.1 eV can be assumed for all measurements. Peak intensity was calculated from the respective peak areas after background subtraction and spectrum fitting by a combination of Gaussian/Lorentzian functions. Energy-dispersive X-ray analyses (EDX) were coupled to the scanning electron microscopy (SEM) LEO Mod. 440 equipment. Ti-K-XANES experiments were performed at the XAS1 beamline of the LNLS (Laboratorio Nacional do Luz Síncrotron, Campinas, São Paulo, Brazil). To evade hydration of the pre-dehydrated samples the analysis was done in a vessel hermetically preserved. TEM were recorded in a JEOL 2100F microscope operated with an accelerating voltage of 200 kV (point resolution of 0.19 nm). JASCO 5300 FTIR spectrometer was used for the FTIR measurements. A thermostatized cell with a special NaBr window warmed up to 400 °C and 4.2×10^{-2} Torr during 2 h was employed to avoid the possible hydration of the samples. The fingerprint of the samples was obtained using wafers of the samples in NaBr.

2.3. Catalytic experiments

The catalytic activity was measured in a batch reactor, fitted with condenser and magnetic stirrer. In order to perform the reactions at 60 °C (unless otherwise specified), the reactor was immersed in a thermostatically controlled water bath at atmospheric pressure. Once the water bath was stabilized at the desired reaction temperature, the feed was added to the reactor. The model feed consisted of 0.2 wt.% of the sulfur-compound (DBT, 98.5% FLUKA; 4,6-DMDBT, 99% Aldrich; BT(98%) Alfa Aesar) in acetonitrile in the L–S phase system and in dodecane-acetonitrile in the L–L–S phase system. Oxidant (hydrogen peroxide (30 wt.%)) and catalyst (100 mg) were then introduced into the reactor with vigorous stirring. The conversion of the S-compound was calculated checking for the remaining sulfur in both phase systems: L–S and L–L–S. In the L–L–S phase system, the resulting mixture was stirred vigorously for a predetermined time at a constant temperature. After each reaction, samples from the oil phase were withdrawn and injected at room temperature to a GC HP 5890 Series II with a HP-5 column and connected to FID and PFPD detectors. *n*-Decane was used as external standard. Oxidized products from polar acetonitrile were confirmed by GC–mass spectroscopy (HP5890) and compared with available standard compounds where available. The H_2O_2 content was measured by standard iodometric titration.

3. Results and discussion

3.1. Characterization of the catalysts

3.1.1. XRD

In Figs. 1 and 2 we can observe de XRD patterns of titanium-modified SBA-16 samples. The XRD pattern of calcined SBA-16 sample shows the typical peaks of (1 1 0) reflection at 1.2° 2θ and two small shoulders of the (2 0 0) and (2 1 1) reflections at 1.7° and 1.92° 2θ, respectively. The calculated a_0 value of 12.16 nm (Table 1) confirmed the Im3m structure [51–55].

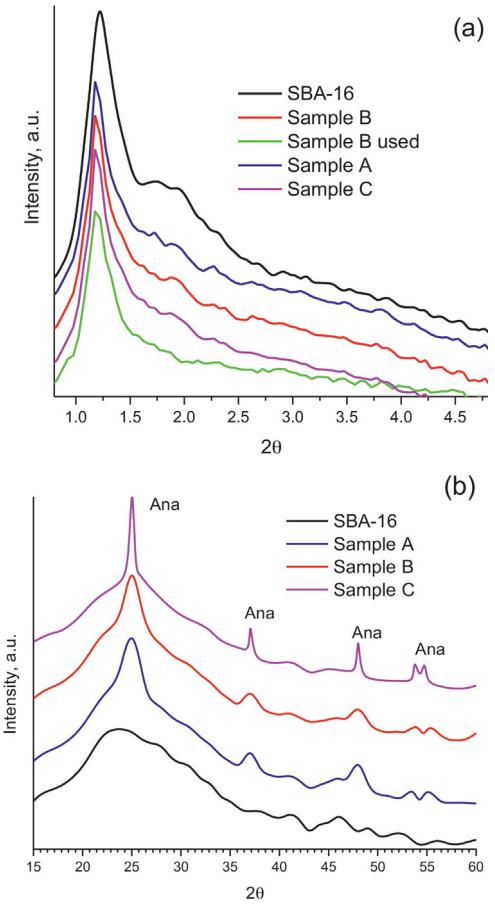

Fig. 1. XRD pattern of TiO_2/SBA-16 synthesized samples: (a) small-angles and (b) wide-angle.

The XRD patterns of TiO_2/SBA-16 (samples A, B and C) are shown in Fig. 1(a) suggesting that the TiO_2 content does not change substantially the XRD pattern, retaining the characteristic SBA-16.

Fig. 1(b) of TiO_2/SBA-16 (samples A, B and C) in the wide-angle range shows a similar pattern that pure anatase phase (Ana). The broadness of the peaks indicate small size of the TiO_2 nanoparticles with the exception of sample C, having the higher TiO_2 content, showing a sharp signal indicating a greater size of the anatase

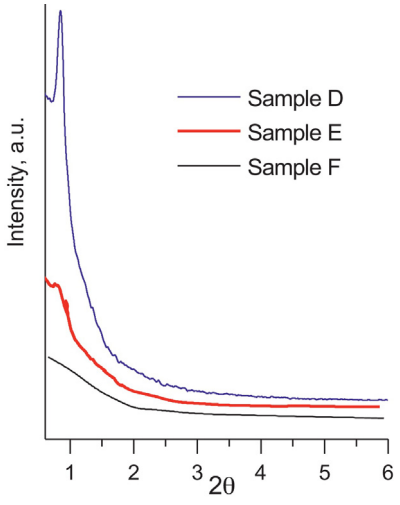

Fig. 2. XRD pattern of Ti-SBA-16 synthesized samples.

Table 1
Physicochemical and structural properties of the catalysts.

	a_0 (nm)	Area (m^2/g)	Ti (wt.%)[a]	Crystal size (μm)[b]	pD (nm)[c]
SBA-16	12.16	870	–	3.50	5.30
TiO_2/SBA-16(A)	12.68	580	4.80[d]	3.43	5.00
TiO_2/SBA-16(B)	12.70	550	6.30[d]	3.42	4.90
TiO_2/SBA-16(C)	12.76	500	8.00[d]	3.40	4.81
Ti-SBA-16(D)	12.80	620	6.72	3.44	5.32
TiO_2	–	95	–	0.05	–

[a] Data obtained by ICP.
[b] SEM.
[c] Average pore diameter determined from the adsorption isotherms by the BJH method.
[d] 15, 20 and 26 wt.% nominal TiO_2 content.

aggregates. It suggests that no large TiO_2 particles are formed outside SBA-16 during the inclusion process (samples A and B), unlike sample C, which appears to have larger particles in the outer surface of SBA-16.

Applying the Scherrer diffraction formula, the size of the TiO_2 nano-crystal was calculated. The values obtained close to 4 nm for samples A and B and 5.8 nm for sample C indicate that the limited pore channels of SBA-16 (about 6 nm) restricted the growth of TiO_2 nanoparticles. This is remarkable in samples A and B, but with higher TiO_2 content, part of the clusters grows out of the pores outside surface. These results are in agreement with the structural properties of the samples (Table 1) and XPS and EDX results (Table 2). A pattern for sample B used after four catalytic tests were added in Fig. 1(a) demonstrating that the structure remains unchangeable.

Fig. 2 probes the substitution of Ti^{4+} for Si^{4+} in the framework location of Ti-SBA-16 (sample D) through a shift of the characteristic signals of SBA-16 to lower 2θ values and evidencing an increase in the unit cell parameters (Table 1).

In the case of the samples with higher content of Ti (samples E and F), the characteristic signal in the plane 100 of SBA-16 is very wide and very poorly defined, this can be explained in terms of a collapse in the structure by higher titanium insertion, results are consistent with Shah et al. [46].

For comparison, Fig. 3 shows the XRD of a pure anatase prepared by us.

Table 1 shows the physicochemical and structural properties of the supports and catalysts. The unit cell parameter of the SBA-16 materials is in good agreement with those reported by others [32,35]. The cubic Im3m pore arrangement and the long-range mesopore architecture were also confirmed by TEM (Fig. 9). The content of titanium in the catalysts was determined by ICP. Metal incorporation and anatase cluster, inside the mesopore of the host, did not disturb the mesopore ordering of SBA-16 materials. As expected, by introducing Ti, a slight decrease in specific surface area (SBET) and average pore diameter was noted for TiO_2/SBA-16 samples, whereas for Ti-SBA-16 average pore diameter was increased due to the longer Ti—O bond than Si—O bond in de host.

Rayo et al. [56] studied the effect on the structural stability of SBA-15 when the NiMo-SBA-15 catalytic materials were

Table 2
Characteristics of Ti species obtained by XPS and EDX of Ti-SBA-16 and TiO_2/SBA-16 catalysts.

Sample	XPS	EDX Atomic ratio	
Ti-SBA-16(D)	$Ti2p_{3/2}$ = 459.4	Si/Ti = 454	Si/Ti = 23.7
TiO_2/SBA-16(A)	$Ti2p_{3/2}$ = 458.5	Si/Ti = 360	Si/Ti = 31.5
TiO_2/SBA-16(B)	$Ti2p_{3/2}$ = 458.5	Si/Ti = 354	Si/Ti = 26.0
TiO_2/SBA-16(C)	$Ti2p_{3/2}$ = 458.55	Si/Ti = 240	Si/Ti = 20.2
TiO_2/SBA-16(B)[a]	$Ti2p_{3/2}$ = 458.5	Si/Ti = 390	Si/Ti = 26.4

[a] Used after four operation cycles.

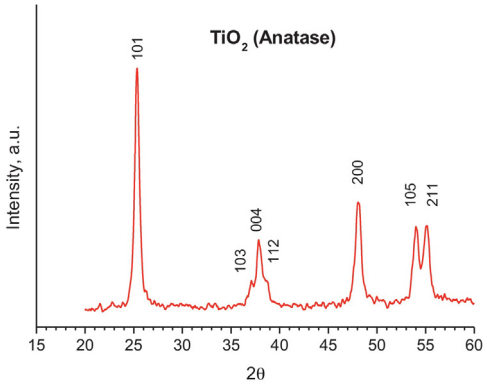

Fig. 3. XRD pattern of TiO_2 as anatase phase.

prepared under different pH conditions. They demonstrated that the mesoporous structure of SBA-15 was preserved after the introduction of the different active sites at lower pH. In our case, the incorporation of titanium species via the post-synthesis method to obtain TiO_2/SBA-16 was adding a solution of titanium-tetrabutyl-orthotitanate in ethanol to the raw SBA-16. The pH of the resultant solution was slightly acid, and some polymerization of terminal silanols could be responsible for the observed reduction of area, but the framework of silica SBA-16 is preserved after the treatment, in agreement with Rayo et al. [56].

3.1.2. FTIR

Fig. 4 shows the FTIR of the anatase prepared by us compared with pure rutile. In the low frequency region, the appearance of a large broad band in the range 400–1000 cm^{-1} maximized at 647 cm^{-1} is characteristic of Ti—O—Ti anatase structure [57]. When both phases are present, bands at 500 cm^{-1} and 617 cm^{-1} (anatase + rutile) are observed. The band at 500 cm^{-1} can be

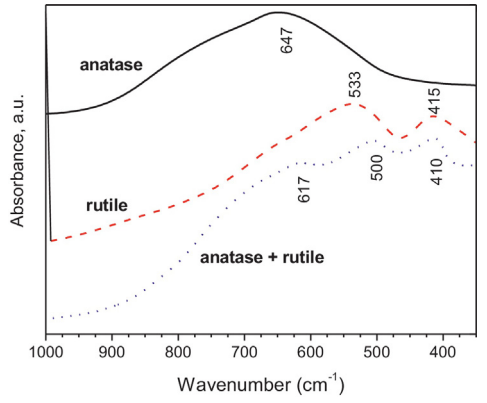

Fig. 4. FTIR of the fingerprint of: anatase, rutile and anatase + rutile samples.

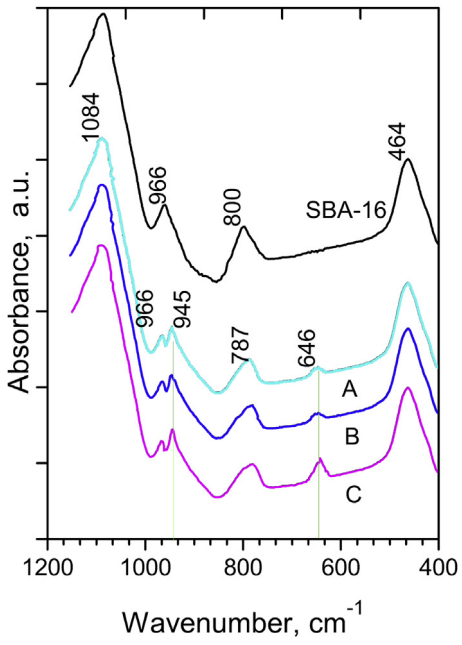

Fig. 5. FTIR of SBA-16 and TiO_2/SBA-16 samples between 1200 and 400 cm^{-1}.

assigned to rutile and 617 cm^{-1} to anatase, both of which shift to lower frequency compared with pure anatase (647 cm^{-1}) or of pure rutile (533 cm^{-1}) by the effect of the first and second coordination sphere of Ti in the sample with both phases.

For SBA-16 and TiO_2/SBA-16 samples the asymmetric stretching vibrations of Si—O—Si band appears at 1084 cm^{-1}. The absorption peaks at 800 and 464 cm^{-1} are due to the symmetric stretching vibration of Si—O—Si band. In addition, the peak at 966 cm^{-1} is indicative of the presence of surface silanol groups [58]. On the other hand, some shifts in the peaks at 945 and 787 cm^{-1} are observed after anatase incorporation (Fig. 5). One shift peak at 945 cm^{-1} is attributed to the combination of the stretching modes of the Si—O^- species in Si—O—Ti^{4+} sequences involving tetrahedral coordinated Ti^{4+} ions [59]. The other shift peak at 787 cm^{-1} is due to the combination of the stretching modes of Si—O—Si and Ti—O—Ti. These features indicate the existence of Si—O—Ti binding between SBA-16 and TiO_2 species. The shift of this band becomes more visible as the incorporation of TiO_2 into SBA-16 increases (samples A, B and C). A more pronounced shift is observed in SBA-16 with 26 wt.% of TiO_2 (sample C). A low frequency band at 646 cm^{-1} attributed to Ti—O—Ti is ascribed to pure anatase, more evident in sample C with higher TiO_2 content.

In view of the FTIR data and according to [60], the best dispersion of titanium, as a function of the contribution of the Si—O—Ti entities is with a content of 20 wt.% TiO_2 in sample B.

3.1.3. UV–vis diffuse reflectance spectroscopic analysis

The chemical environment and dispersion of titanium heteroatom incorporated in the silica matrix of SBA-16 was determined by UV–vis diffuse reflectance spectroscopy. The spectra of the catalyst synthesized with different method and different content of titanium are shown in Fig. 6. As we determined in our previous work [49], the bands at 210, 240–320 and 320–400 nm, correspond to isolated framework Ti (IV), octahedral coordinated Ti species, and titania (anatase) phase, respectively [61–63]. Ti-SBA-16 (sample D) has the band only at 210 nm, assigned to mono-atomically dispersed Ti^{4+} ions, this fact suggests the presence of tetrahedral isolated Ti ions [62]. The spectra of TiO_2/SBA-16 different samples are also shown in Fig. 6. The shift of the absorption band of samples A and B to shorter wavelength range, indicates that

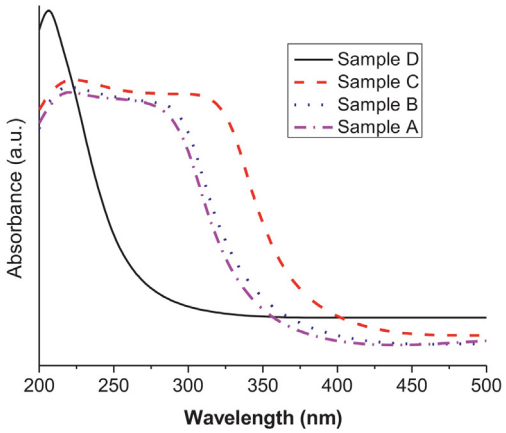

Fig. 6. UV–vis diffuse reflectance spectra of Ti-SBA-16 and TiO_2/SBA-16.

the size of the pore channels of the framework avoid the growing of the TiO_2 particles, obtaining a small size of the crystal of anatase within SBA-16. Upon increasing TiO_2 content (sample C) a shift in the UV to higher wavelengths of the absorption edge is observed, indicating the growth of the nanodomains as titania. The data are in agreement with the XRD patterns.

3.1.4. Raman

For SBA-16, Raman bands at 430, 800 and 1080 cm^{-1} are observed in Fig. 7. The bands at 430 and 1080 cm^{-1} can be attributed to symmetric and asymmetric vibrations of the Si—O—Si unit, respectively. The band at 800 cm^{-1} is the symmetric stretching

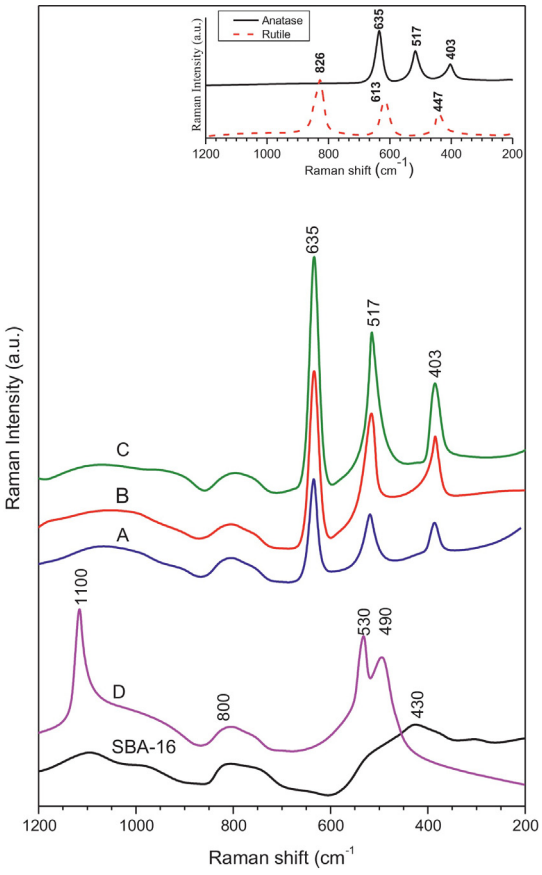

Fig. 7. Raman spectra of SBA-16, Ti-SBA-16 and TiO_2/SBA-16. Inset: rutile and anatase.

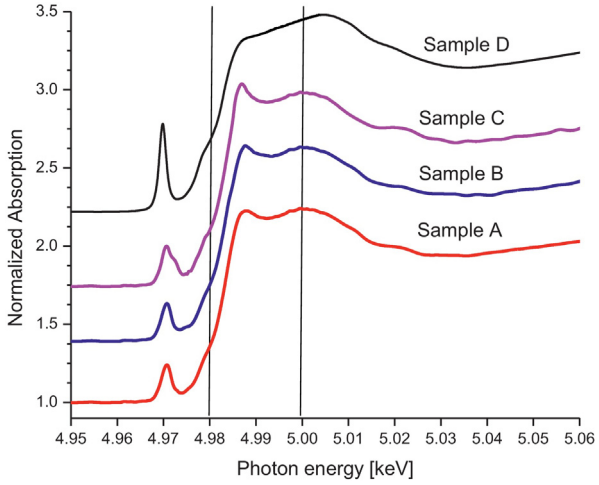

Fig. 8. XANES spectra of Ti-SBA-16 and TiO_2/SBA-16. Pre-peak region (PPR), white line region (WLR).

mode of the tetrahedral [SiO_4] unit [64–66]. In addition to these bands, three new bands at 490, 530 and 1110 cm^{-1} are observed for Ti-SBA-16 (sample D). The bands at 490 and 530 cm^{-1} are ascribed to the bending and symmetric stretching vibration of the framework Ti—O—Si species, respectively. The band at 1110 cm^{-1} is due to the relatively flexible symmetric vibration of tetrahedral coordinated [$Ti(OSi)_4$] units in SBA-16 [67], similar to that found in SiO_2 surface.

Fig. 7 also shows the spectra of TiO_2/SBA-16 (samples A, B and C), the characteristic signals of anatase are detected in the three samples if we compare with pure anatase [63] and pure rutile [64] bands, present in the inset of the figure. This fact demonstrates that titanium is incorporated mainly as anatase phase.

3.1.5. XPS

XPS analysis of the catalysts is listed in Table 2. In the spectra (not shown) Ti appears as Ti^{+4} (—O_4—) $Ti2p_{3/2}$ = 459.4 eV due to the isomorphous Si substitution in Ti-SBA-16. Hence for TiO_2/SBA-16 (samples A, B and C), the Ti $2p_{3/2}$ = 458.5 eV signal indicate that Ti is incorporated in the mesoporous nanostructure of SBA-16, as anatase phase [60,68].

The atomic ratio of Si/Ti (360 and 354) for TiO_2/SBA-16 (samples A and B) shown in Table 2, indicate that Ti species are well dispersed in the mesopores of SBA-16 due to the low signal observed in XPS analysis (100 Å of depth) most of which is within the pore nanostructure. However, for TiO_2/SBA-16 (sample C), a slight decrease Si/Ti (240) is observed, supporting the idea that for this sample, some of TiO_2 species are on the external surface of the support. This is confirmed by the very low Si/Ti ratios obtained by EDX (Table 2). It should be noted that after four catalytic cycles of reaction for TiO_2/SBA-16 (sample B) (the best catalyst as we will show later), XPS and EDX results indicate an almost imperceptible disappearance of Ti; thus, no leaching of titanium from the support can be assumed.

3.1.6. XANES

The electronic transitions evidenced by Ti-K XANES experiments are useful to analyze Ti coordination. Fig. 8 clearly shows the variation in both, intensity and spectra position in the pre-peak region (4.96–4.98 keV) and in the white line region (4.98–5.0 keV). Features of the XANES Ti-K edge spectra of the Ti-containing SBA-16 samples studied indicates that Ti(IV) ions have an octahedral surrounding, typical of anatase-like structure for TiO_2/SBA-16 samples. As TiO_2 increases (sample C), the absorption band assigned to 1s-to-3d transitions at 4.972 keV appears as a doublet with the band at 4.970 keV of the other sample with lower anatase content, according to the higher absorption band at 4.985 keV assigned to 3s-to-np dipole transitions. These two differences between the lower and the higher titania content are due to the fact that some nano species of TiO_2 possess an intensive absorbance. Thus, in sample C, pure anatase is probably scattered and disturbed by the network of silica SBA-16. On the other hand, the indication in favor of the presence of Ti(IV) ions with a lower oxygen coordination surrounding (tetrahedral) has been obtained for Ti-SBA-16 (sample D). Thus, XPS, UV–vis DRS, FTIR and Raman data are in agreement with XANES results.

3.1.7. TEM

The morphological characterization of titanium particles in TiO_2, Ti-SBA-16 and TiO_2/SBA-16 was examined by means of transmission electron microscopy (TEM), see Fig. 9. In Fig. 9a, the synthesized nanoparticles of anatase appear to have variable flat and ellipsoidal shapes with individual nanoparticles ranging from 40 to 60 nm, particularly higher than TiO_2 species formed in the mesopore of TiO_2/SBA-16 samples. Fig. 9b shows TEM image for TiO_2/SBA-16 (sample B); it clearly depicts the formation of a high quality 3-D channel through the perpendicular. Pores (clear zones) and TiO_2 particles (darker zones) allow determining a particle size distribution ranging from ~4 to 5 nm for TiO_2 particles (sample B). This fact indicates that most TiO_2 particles were present inside the pores, in agreement with XPS and EDX data shown in Table 2. This result strongly suggests that SBA-16 acts as a nanoreactor, suppressing with effectiveness of the growth of TiO_2 particles, as supported by the rest of the characterization results shown above. In Fig. 9c we can see the image of the TiO_2/SBA-16 (sample B) used after four operation cycles, where the highly ordered mesopore structure is manifest, which has not evidently suffered the clogging of the mesopore channels by TiO_2 particles or other adsorbed sulfur-containing compounds. The image of Ti-SBA-16 (sample D) shows a three-dimensional body-centered cubic (bcc) cage-like interconnected mesopore structure as pure siliceous SBA-16 (Fig. 9d).

3.2. Catalytic activity

We tested sulfur removal of different desulfurization systems. In the adsorption process, when bare mesoporous SBA-16 sample was used as the adsorbent for desulfurization from model feed, the DBT removal was only 3.0%. Low conversion of DBT in presence of H_2O_2 (H_2O_2/S = 5) was obtained in the absence of the catalyst (less than 8% at 70 °C). This result indicated that the blank experiment without catalyst and with pure support (SBA-16) show very low conversion and the Ti-species present in SBA-16 play the main role in the catalytic activity. Fig. 10 shows the catalytic results from the ODS of DBT using the different synthesized catalysts (TiO_2, TiO_2/SBA-16 and Ti-SBA-16) in a liquid–solid (L–S) phase system. DBT was oxidized to it sulfone (100% yields); sulfoxide or other products were not detected in the conditions studied. From the figure, we can note that at 30 min of reaction time, TiO_2/SBA-16 (sample B) displays a DBT conversion 20% higher than that of Ti-SBA-16 (sample D), and 4 times higher than that of TiO_2. TiO_2/SBA-16 catalysts (samples A and C), with lower and higher Ti content, respectively, were less active than TiO_2/SBA-16 (sample B), with an intermediate Ti content. In the case of sample A, which could be explained in terms of number of active sites exposed, and in the case of TiO_2/SBA-16 (sample C), some part of the titanium forms anatase cluster of higher size outside the pores, decreasing the surface area exposed to the reactants. DBT removal from a 0.2 wt.% solution in acetonitrile was as high as 90% within 50 min reaction for TiO_2/SBA-16 (sample B). The superior DBT desulfurization of this material suggests a determining effect on TiO_2 species critical size, with greater

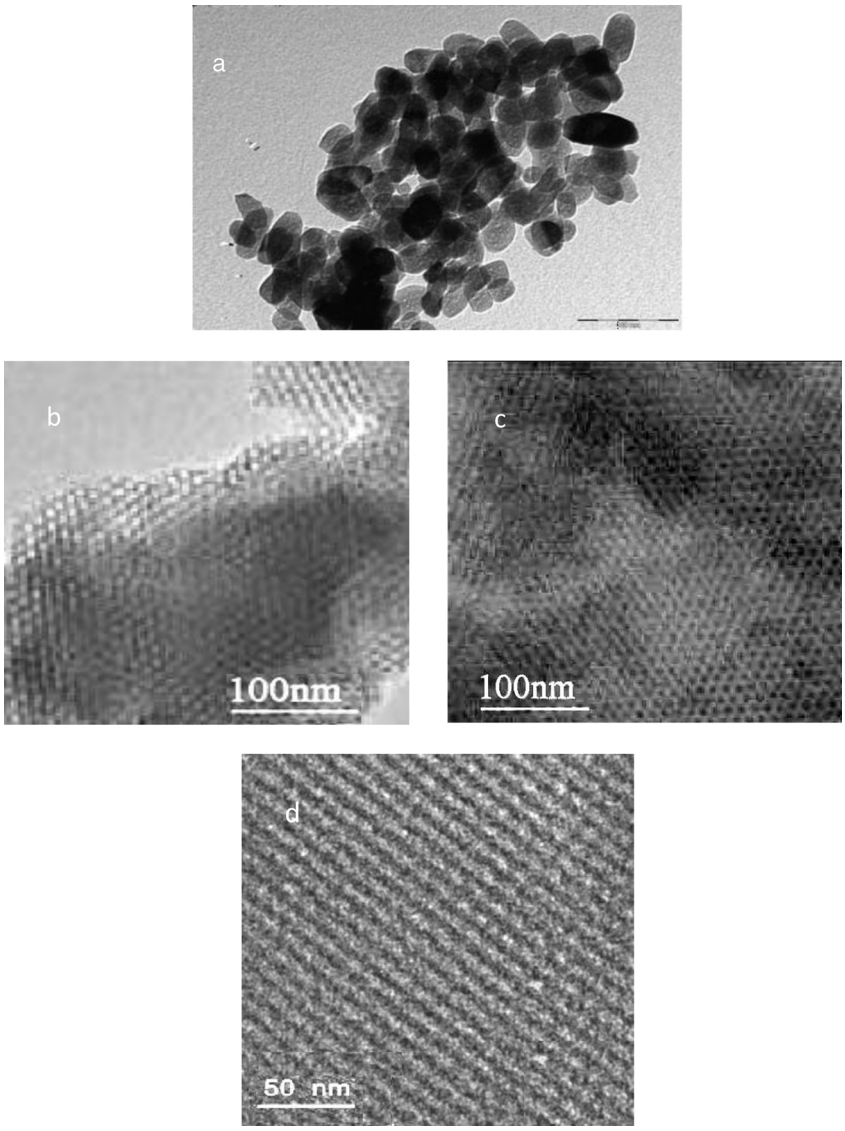

Fig. 9. TEM images of: (a) TiO_2, (b) TiO_2/SBA-16 sample B, (c) sample B used and (d) Ti-SBA-16 (sample D).

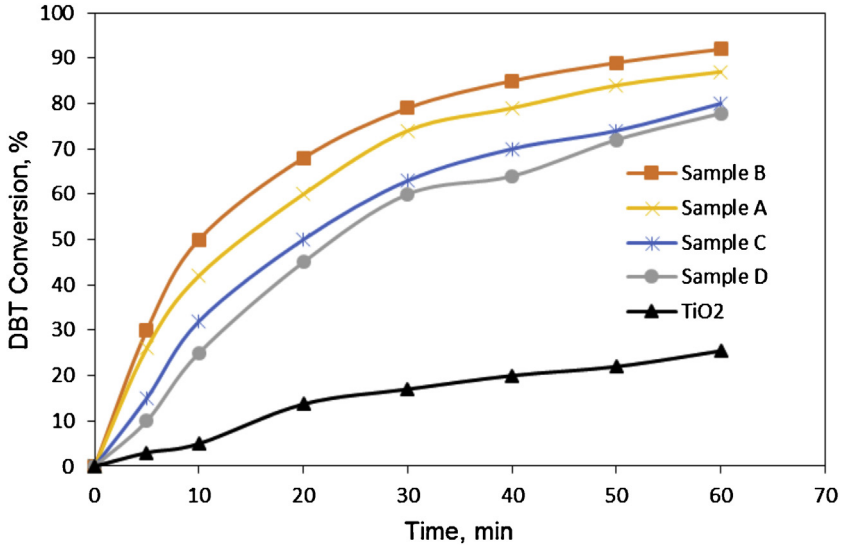

Fig. 10. DBT conversion for the different catalysts. Molar ratio H_2O_2/DBT = 5, g DBT/g cat = 1, T = 60 °C.

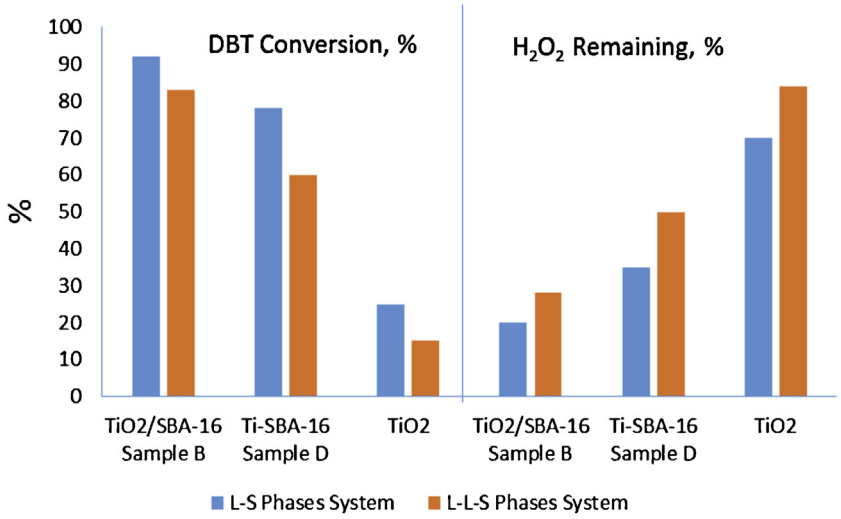

Fig. 11. DBT conversion (left) and H_2O_2 remaining (right) after ODS reaction, with TiO_2/SBA-16, Ti-SBA-16 and TiO_2 in L–S phase system (acetonitrile as polar phase) and in L–L–S phases system (acetonitrile as polar phase and dodecane as oil phase). Molar ratio H_2O_2/DBT = 5, g DBT/g cat = 1, T = 60 °C. Reaction time = 60 min.

exposed surface area. Is estimated that, TiO_2 supported on SBA, is the most active site for DBT oxidation. Hydrogen peroxide and TiO_2-active species form an intermediate that reacts with sulfur compound adding oxygen-atom into the sulfur atom of the DBT.

The effect of mass transfer was studied comparing two different phase systems. We present a three-phase liquid–liquid–solid (L (oil)–L (solvent)–S (catalyst) system, where the proposed mechanism for the catalytic oxidation of DBT in the reaction occurs by simultaneous extraction/oxidation of dibenzothiophene in acetonitrile solution, wherein is the catalyst and H_2O_2. Ti surface sites in the catalysts are capable of interacting with H_2O_2 to produce large amounts of superoxide radical. These radical species can oxidize the DBT molecules in acetonitrile phase to their corresponding sulfones (DBTO2), and hence polar DBTO2 do not migrate into the oil phase. The catalytic cycle can take place multiple times under low H_2O_2 concentration and low temperature conditions. If the liquid–liquid extraction step does not occur rapidly, the transfer of DBTs from the oil phase to the solvent phase will affect the rate of the global process.

In order to demonstrate the effect of mass transfer, a comparison was made between the L–S and L–L–S phase systems (with dodecane as solvent in the oil phase and acetonitrile in the solvent phase).

Fig. 11 exhibits the results yielded. A better conversion was obtained in the L–S phase system for all the samples, probing the existence of mass transfer limitation. Therefore, to obtain kinetic parameters in the subsequent experiments we will use a two phase-system.

Additionally, the percentage of H_2O_2 remaining after reaction was determined by titration (Fig. 11).

TiO_2/SBA-16 (sample B) presents the higher ODS activity, compared with Ti-SBA-16 (sample D), which gives account of the greater consumption of oxidant during oxidation. On the basis of the results observed we assume that the structure of the Ti site in TiO_2/SBA-16 is more capable than that of Ti-SBA-16 of decomposing H_2O_2 to form the Ti-peroxo complex which gives the active oxygen species needed in the formation of the DBT-sulfone. In the case of pure TiO_2, more than 70% of the oxidant remains in the system after reaction time, suggesting that this catalyst is unable to fully decompose the peroxide.

Previous literature results [26,44,64] claimed that Ti in tetrahedral position as in Ti-SBA-16 would present high activity; yet contrary to what we expected, Ti-SBA-16 was less active than TiO_2/SBA-16. Although extra-framework TiO_2 was expected to decompose and consume much H_2O_2 during oxidation, this was not evidenced in the TiO_2/SBA-16 sample, as seen in Fig. 11. This may be attributed to the small size of well dispersed TiO_2 particles, confined within the pores of the support, making a more active catalytic site. Fig. 11 also shows that TiO_2/SBA-16 is slightly more hydrolytically stable toward aqueous H_2O_2 than Ti-SBA-16. Ti-SBA-16 presents an intermediate activity probably resulting from the fact that Ti—O—Si isolated species are not always exposed to reactants, thus having lower activity.

Cedeño-Caero et al. [40] compared the ODS of dibenzothiophene between titanium oxide nanotubes and a titanium-substituted mesoporous SBA-15 molecular sieve using commercial titanias as a reference. In that work Ti-SBA-15 (19 wt.% of TiO_2), titanium oxide nanotubes and the commercial TiO_2, which are titanium compounds (trititanate and TiO_2-anatase), achieved 90, 62 and 23% of DBT-sulfone yield, respectively. The isolated Ti species linked to Si atoms through oxygen bridges in Ti-SBA-15 displayed an activity lower than that of TiO_2 particles; thus it was concluded that TiO_2 was the main active phase in the catalysts studied. The results reported here are in agreement with those in Cedeño-Caero et al. [40] where the activity of TiO_2-containing catalysts seemed to be directly proportional to the exposed TiO_2 surface area (smaller cluster size and high dispersion).

The XPS data of used TiO_2/SBA-16 (Table 2) showed that titanium leaching is negligible, in addition to the high hydrolytic stability of the structure of this material.

The higher catalytic activity of TiO_2/SBA-16 can be rationalized by taking into account the fact that more titanium sites are more accessible in this material.

We chose the most active catalyst, TiO_2/SBA-16 (sample B), to perform the subsequent experiments aimed studying the effect of several experimental conditions.

The influence of hydrogen peroxide concentration on the conversion of DBT was explored. Different H_2O_2/DBT molar ratios were selected, including 16/1, 10/1, 5/1 and 2.5/1 (Fig. 12). In the stoichiometry of this reaction, only 2 mol of H_2O_2 are consumed per mole of sulfone (R-SO_2) produced. However, the reaction rate increases as the H_2O_2/DBT ratio increases; the reaction rate is the highest for H_2O_2/DBT = 16/1 molar ratio, for which complete DBT conversion was achieved at 25 min. The reaction is favored under excess of hydrogen peroxide. Although the reaction rate is slightly lower with H_2O_2/DBT = 5/1 molar ratio, 90% of DBT conversion can be reached at 60 min. In this way, the H_2O_2/DBT molar ratio was optimized in terms of the high conversion reached at relatively

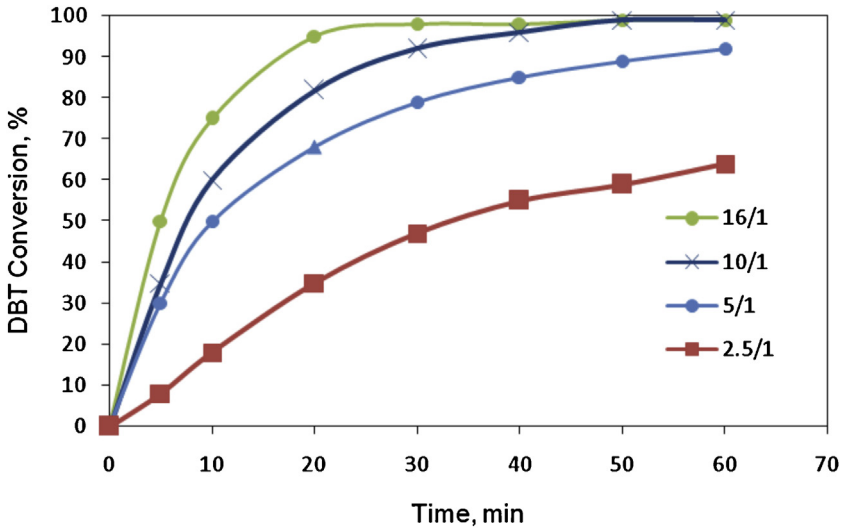

Fig. 12. Effect of H_2O_2/DBT molar ratio in the DBT conversion for TiO_2/SBA-16 in L–S phase system. g DBT/g cat = 1, T = 60 °C.

short time; this ratio is interesting, taking account the economical point of view. A molar ratio of H_2O_2/DBT = 5/1 being used for kinetic calculations. In comparison with other works [25,40,46], we obtained good activities using a lower peroxide/sulfur ratio at milder conditions.

3.3. Kinetic calculations

Here we compared the performance of TiO_2/SBA-16 in the ODS of other sulfur-containing compounds present in middle distillate fuels such as dibenzothiophene (DBT), 4,6-dimethyldibenzothiophene (4,6-DMDBT) and benzothiophene (BT).

In order to gain kinetic information, the kinetics of DBT, 4,6-DMDBT and BT, with TiO_2/SBA-16, was investigated in a L–S phase system. The changes in volume with the samples withdrawal are neglected. As we used an excess of H_2O_2, any variation in concentration could be disregarder. A set of experiments was performed to check the absence of intraparticle and interphase mass transfer limitations. Different sizes of catalyst particles (0.2, 0.4, 0.6) were tested; the results indicated that in all cases a kinetic regime was established. External mass transfer limitation was evaluated changing the stirrer speeds ranging from 200 to 800 rpm to determine the external mass transfer effect. The rate of reaction increases initially with the stirrer speed and this rise is insignificant at or above 300 rpm, indicating the independence of reaction rate on speed. Hence, all the subsequent experiments were performed at 500 rpm.

The main oxidized product is confirmed to be the sulfone for DBT and 4,6-DMDBT and benzothiophenedioxide for BT. Some traces of others unidentified products were detected. It is known that thiophene and benzothiophene are more difficult to oxidize than the DBTs. However, good results on oxidation of benzothiophene, in similar conditions that used in this work, were reported in literature. Maity et al. [39] reported the oxidation of benzothiophene in isooctane with hydrogen peroxide performed in a batch reactor in a non-severe condition using nano-crystalline Ti-beta catalyst. ODS of benzothiophene also showed good results over different Ti-containing molecular sieves [27], Ti-SBA-15 catalyst [14] and Ti-beta and Ti-MCM-41 catalyst using different oxidants [26]. Hazan et al. [21] studied the oxidative desulfurization of model fuel containing 1000 ppm of benzothiophene with WO_x/ZrO_2 catalyst at 60 °C and 30% aqueous H_2O_2 solution (oxidant to sulfur molar ratio (O/S) = 15), and 5 mL of acetonitrile as an extractive solvent. They applied pseudo-first-order rate constants for the benzothiophene oxidation at different temperatures. The good activity of BT was also reported for ODS with MoO_3 catalysts [18,22]. The oxidation of benzothiophene with homogeneous and heterogeneous rhenium catalysts and H_2O_2 has been studied by Di Giuseppe et al. [69]. Excellent results in terms of both conversion and yields of sulfones were obtained. A phosphotungstic acid/activated carbon (HPW/AC) catalyst with H_2O_2 showed good catalytic performance for ODS of model gasoline benzothiophene and thiophenic compounds [70].

The effect of temperature (50, 60, and 70 °C) is shown in Fig. 13(a), (b) and (c), respectively. An increase in the reaction temperature from 50 to 70 °C raised conversion from 50 to 90% for DBT and from approximately 30 to 70% for 4,6-DMDBT and BT, in only 17 min of reaction. This fact is in agreement with previous reports [18,71]. The experimental data obtained for the three S-bearing compounds were fitted to a pseudo-first-order rate equation Eq. (1).

$$\ln\left(\frac{C_0}{C_t}\right) = -kt \quad (1)$$

Here k is the rate constant; C_0 (M) and C_t (M) are the concentrations of sulfur-containing compounds (DBT, 4,6-DMDBT or BT) at 0 min and t (min), respectively. Plots of $\ln(C_t/C_0)$ versus reaction time (t) are shown in Fig. 14; the linear relationships obtained confirm the pseudo-first-order reaction kinetics proposed. As temperature increases, the rate constant increases for all compounds (Table 3).

Table 3
Pseudo-first-order rate constants of the S-compounds oxidation over TiO_2/SBA-16 catalyst at different temperatures.

Temperature (°C)	Rate constant, k (min^{-1})		
	Dibenzothiophene	4,6-Dimethyldibenzothiophene	Benzothiophene
50	0.0400	0.0229	0.0216
60	0.0671	0.0481	0.0438
70	0.1245	0.0775	0.0755

All the correlation factors R^2 are over 0.98.

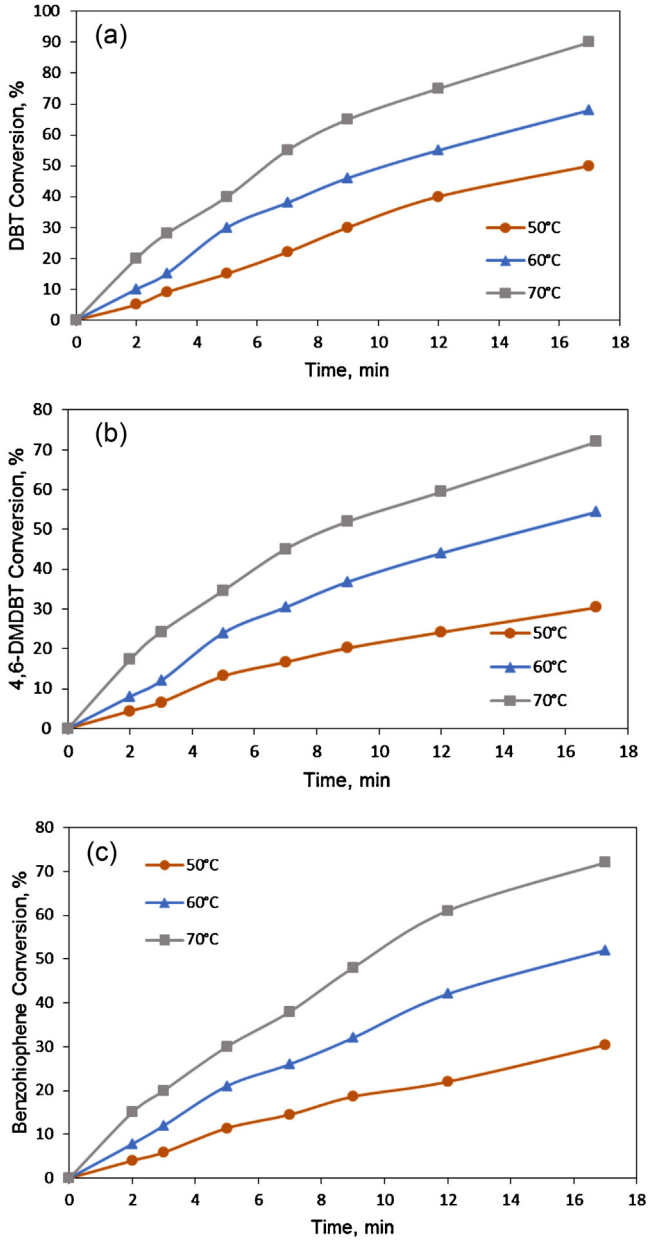

Fig. 13. Effect of reaction temperature vs. time on the conversion of (a) DBT, (b) 4,6-DMDBT and (c) benzothiophene with TiO_2/SBA-16. Molar ratio H_2O_2/S = 5, 0.011 mol of S/0.1 g cat.

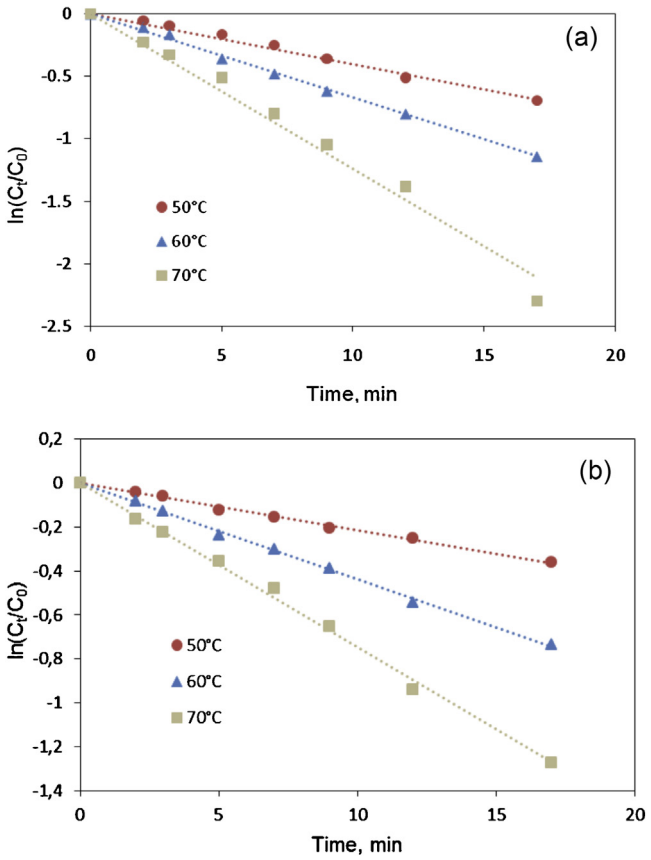

Fig. 14. Plots of the pseudo-first-order kinetics for the oxidation of (a) DBT and (b) 4,6-DMDBT and (c) benzothiophene with TiO_2/SBA-16.

The higher rate constants obtained for DBT, compared with those for 4,6-DMDBT and BT, indicate that the oxidation of DBT is easier than that of the others.

The reaction rate was found to increase as follows: DBT > 4,6-DMDBT > BT. The order should follow the electron densities on sulfur atoms as calculated by Otstuki et al. [13]: 4,6-DMDBT (5.760) > DBT (5.758) > BT (5.739). In that case, 4,6-DMDBT with higher electron density should be rapidly oxidized. However, the shift in the order could be ascribed to the fact that methyl groups represent an obstacle for the adsorption of the sulfur atom to the active site of catalyst [72].

Arrhenius equation (Eq. (2)) expresses the dependence of the rate constant k on the reaction temperature:

$$k = A \exp\left(-\frac{E_a}{RT}\right) \quad (2)$$

where E_a is the apparent activation energy; A is the pre-exponential factor; and R and T are the gas constant and reaction temperature (K), respectively. The Arrhenius plots are shown in Fig. 15. The calculated E_a values for the oxidation of DBT, 4,6-DMDBT and BT are 43.4 kJ/mol, 46.7 kJ/mol and 48.1 kJ/mol, respectively. Therefore, E_a values for BT and 4,6-DMDBT are quite similar and even higher than that for DBT. The high electron density on the S of DBTs favors the electrophilic addition of oxygen. These values are quite similar to those reported in other works; E_a for DBT oxidation was 52.83 kJ/mol using polyoxometalates as catalysts and hydrogen peroxide/acetic as oxidant [73]. Ling et al. [74] reported activation energy of 60 kJ/mo1for DBT oxidation in H_2O_2/formic acid. Hazan et al. [21] applied pseudo-first-order rate constants for the benzothiophene oxidation at different temperatures and they obtained

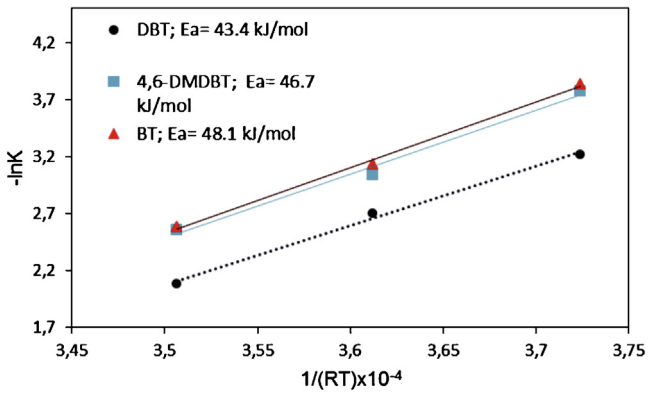

Fig. 15. Arrhenius activation energy for S-compounds oxidation.

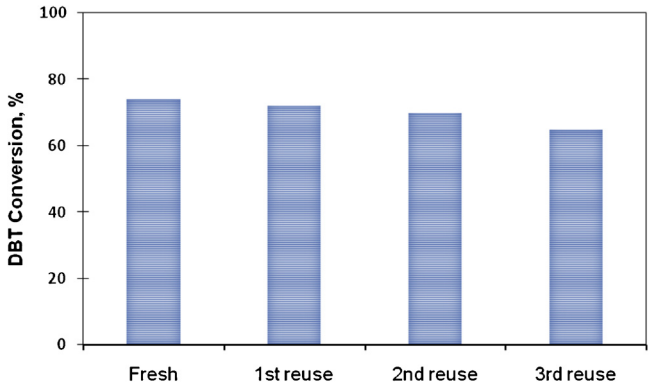

Fig. 16. DBT conversion in several reaction cycles of the TiO_2/SBA-16 catalyst at 60 min of reaction time. Molar ratio H_2O_2/DBT = 5, T = 60 °C, g DBT/g cat = 1.

values similar than that obtained by us, also the calculated E_a for the oxidation of BT was 23.5 kJ/mol.

3.4. Deactivation of the catalyst

The deactivation of a catalyst is very important for industrial feasibility. The reusability of the catalyst for the ODS of DBT has been tested after washing with water–methanol and after washing followed by calcination for 2 h in a muffle furnace at 500 °C. Similar result was obtained with both methods. In Fig. 16 we observe that the activity of the calcined sample remains after the third recycle compared to a fresh catalyst. The purpose of washing with water–methanol is eliminating all oxidized products that could be adsorbed on the catalysts. The regeneration of the catalyst for 2 h in a muffle furnace at 500 °C was made in order to ensure the complete elimination of organic compounds that could block the pores. The hydrolytic stability of the structure of these materials after recycling was confirmed by XRD (Fig. 1) and TEM (Fig. 9). The active sites were unaltered during the reaction, according the Si/Ti analyzed by XPS (Table 2), since leaching of titanium could occur in the studied conditions [75–78]. The results confirm that the catalyst has no changed. This information will be valuable to determine which type of catalyst will be potentially suitable for the ODS of heavy petroleum fractions, where some coke-precursors formation is possible. The reusability of the catalyst indicates that TiO_2/SBA-16 is a potential catalyst, which can be applied to this process.

4. Conclusions

The two methods of Ti incorporation, into a high surface area support, allowed preparation of mesoporous SBA-16 type materials with relatively high Ti and/or TiO_2 loadings, maintaining the initial SBA-16 structure. The preparation of Ti-SBA-16 with high loading of titanium in tetrahedral coordination is limited to a certain proportion (Si/Ti = ~23); with a lower molar ratio, the structure of SBA-16 collapse with the resulting decrease in activity. An adequate preparation of highly Ti loaded catalysts with highly dispersed TiO_2 nano-clusters was possible due to the limitation of the critical molecular space available in SBA-16. Thus, in this paper we demonstrate that TiO_2/SBA-16, without loss of its structure and with a well-dispersed TiO_2 phase, is more active than the Ti-SBA-16 for ODS at mild conditions. The higher catalytic activity of TiO_2/SBA-16 can be explained by considering that more dispersed titanium sites are accessible in this material. In addition, no loss of catalytic activity was observed after recycling, thus confirming the hydrolytic stability of TiO_2/SBA-16 materials.

Acknowledgments

The authors are very grateful to Drs. J.L. García Fierro, J.M. Martin and H. Falcon for XPS, UV–vis DRS characterization performed in ICP-CSIC, Madrid.

We thank CONICET Argentina, PIP CONICET 11220120100218CO (2013–2016), and MINCyT Cba, 1210/07 (2014–2016) for financial assistance.

References

[1] J. Xiao, L. Wu, Y. Wu, B. Liu, L. Dai, Z. Li, Q. Xia, H. Xi, Appl. Energy 113 (2014) 78.
[2] O. Gonzalez-Garcia, L. Cedeño-Caero, Catal. Today 150 (2010) 237.
[3] X. Chen, D. Song, C. Asumana, G. Yu, J. Mol. Catal. A: Chem. 359 (2012) 8.
[4] W.A. Bakar, R. Ali, A.A. Kadir, W.N. Mokhtar, Fuel Process. Technol. 101 (2012) 78.
[5] H. Shang, H. Zhang, W. Du, Z. Liu, J. Ind. Eng. Chem. 19 (2013) 1426.
[6] E. Rafiee, S. Eavani, J. Ind. Eng. Chem. 380 (2013) 18.
[7] Z. Eldin, A. Abdalla, B. Li, Chem. Eng. J. 200–202 (2012) 113.
[8] A. Stanislaus, A. Marafi, M.S. Rana, Catal. Today 153 (2010) 1.
[9] Y. Shiraishi, K. Tachibana, T. Hirai, I. Komasawa, Ind. Eng. Chem. Res. 41 (2002) 4362.
[10] E.W. Qian, J. Jpn. Petrol. Inst. 51 (2008) 14.
[11] J.M. Campos-Martin, M.C. Capel-Sanchez, P. Perez-Presas, J.L.G. Fierro, J. Chem. Technol. Biotechnol. 85 (2010) 879.
[12] H. Gomez, L. Cedeño, Int. J. Chem. React. Eng. 3 (2005) A28.
[13] S. Otsuki, T. Nonaka, N. Takashima, W. Qian, A. Ishihara, T. Imai, T. Kabe, Energy Fuels 14 (2000) 1232.
[14] D. Wang, E.W. Qian, H. Amano, K. Okata, A. Ishihara, T. Kabe, Appl. Catal. A: Gen. 253 (2003) 91.
[15] I.V. Babich, J.A. Moulijn, Fuel 82 (2003) 607.
[16] A. Akbari, M. Omidkhah, J.T. Darian, Ultrason. Sonochem. 21 (2014) 692.
[17] Y. Nie, Y. Dong, L. Bai, H. Dong, X. Zhang, Fuel 103 (2013) 997.
[18] M.C. Capel-Sanchez, P. Perez-Presas, J.M. Campos-Martin, J.L.G. Fierro, Catal. Today 157 (2010) 390.
[19] G.-N. Yun, Y.-K. Lee, Fuel Process. Technol. 114 (2013) 1.
[20] E. Torres-García, A. Galano, G. Rodriguez-Gattorno, J. Catal. 282 (2011) 201.
[21] Z. Hasan, J. Jeon, S.H. Jhung, J. Hazard. Mater. 205–206 (2012) 216–221.
[22] Y. Jia, G. Li, G. Ning, Fuel Process. Technol. 92 (2011) 106.
[23] E. Ito, J.A.R. van Veen, Catal. Today 116 (2006) 446.
[24] V. Hulea, A.L. Maciuca, F. Fajula, E. Dumitriu, Appl. Catal. A: Gen. 313 (2006) 200.
[25] L. Cedeño-Caero, H. Gomez-Bernal, A. Fraustro-Cuevas, H.D. Guerra-Gómez, R. Cuevas-García, Catal. Today 133–135 (2008) 244.
[26] A. Chica, A. Corma, M.E. Domine, J. Catal. 242 (2006) 299.
[27] V. Hulea, F. Fajula, J. Bousquet, J. Catal. 195 (2001) 179.
[28] L.C. Caero, E. Hernandez, F. Pedraza, F. Murrieta, Catal. Today 107–108 (2005) 564.
[29] Y. Shiraishi, T. Naito, T. Hirai, Ind. Eng. Chem. Res. 42 (2003) 6034.
[30] A.V. Anisimov, E.V. Fedorova, A.Z. Lesnugin, V.M. Senyavin, L.A. Aslanov, V.B. Rybakov, A.V. Tarakanova, Catal. Today 78 (2003) 319.
[31] E. Torres-Garcia, G. Canizal, S. Velumani, L. Ramirez-Verduzco, F. Murrieta-Guevara, J. Ascencio, Appl. Phys. A: Mater. Sci. Process. 79 (2004) 2037.
[32] B. Zapata, F. Pedraza, M.A. Valenzuela, Catal. Today 106 (2005) 219.
[33] D. Srinivas, P. Ratnasamy, Microporous Mesoporous Mater. 105 (2007) 170–180.
[34] P. Rayo, J. Ramírez, M.S. Rana, J. Ancheyta, A. Aguilar-Elguézabal, Ind. Eng. Chem. Res. 48 (2009) 1242–1248.
[35] L.Y. Kong, G. Li, X.S. Wang, Catal. Today 93–95 (2004) 341.
[36] L.Y. Kong, G. Li, X.S. Wang, Catal. Lett. 92 (2004) 163.
[37] B. Li, Z. Liu, J. Liu, Z. Zhou, X. Gao, X. Pang, H. Sheng, J. Colloid Interface Sci. 362 (2011) 450.
[38] U. Arellano, J.A. Wang, M.T. Timko, L.F. Chen, S.P. Paredes Carrera, M. Asomoza, O.A. González Vargas, M.E. Llanos, Fuel 126 (2014) 16.
[39] U. Maity, J. Kumar Basu, S. Sengupta, Fuel 113 (2013) 180–186.
[40] L. Cedeño-Caero, M. Ramos-Luna, M. Mendez-Cruz, J. Ramirez-Solis, Catal. Today 172 (2011) 189.
[41] E. Lorençon, D. Alves, K.E. Krambrock, S. Ávila, R.R. Resende, A.S. Ferlauto, R.M. Lag, Fuel 132 (2014) 53.
[42] A. Corma, M. Iglesia, F. Sanchez, Catal. Lett. 39 (1996) 153.
[43] T.W. Kim, M.J. Kim, F. Kleitz, M.M. Nair, R.G. Nicolas, H.J. Jeong, C. Chae, U. Kim, S.Y. Jeong, ChemCatChem 4 (2012) 687.
[44] K.-S. Cho, Y.-K. Lee, Appl. Catal. B 147 (2014) 35.
[45] N.N. Trukhan, V.N. Romannikov, A.N. Shmakov, M.P. Vanina, E.A. Paukshtis, V.I. Bukhtiyarov, V.V. Kriventsov, I.Yu. Danilov, O.A. Kholdeeva, Microporous Mesoporous Mater. 59 (2003) 73.
[46] A.T. Shah, B. Li, Z. Eldin, A. Abdalla, J. Colloid Interface Sci. 336 (2009) 707.
[47] Y. Sakamoto, M. Kaneda, O. Terasaki, D.Y. Zhao, J.M. Kim, G. Stucky, H.J. Shin, R. Ryoo, Nature 408 (2000) 449.

[48] G.S. Balangero Bottazzi, M.L. Martinez, M. Gomez Costa, O.A. Anunziata, A.R. Beltramone, Appl. Catal. A 404 (1–2) (2011) 30.
[49] B.C. Ledesma, V.A. Valles, L.P. Rivoira, M.L. Martinez, O.A. Anunziata, A.R. Beltramone, Catal. Lett. 144 (2014) 783.
[50] T.W. Kim, R. Ryoo, M. Kruk, K. Gierszal, K.M. Jaroniec, S. Kamiya, O. Terasaki, J. Phys. Chem. B 108 (2004) 11480.
[51] D. Zhao, J. Feng, Q. Huo, N. Melosh, G.H. Fredrickson, B.F. Chmelka, G.D. Stucky, Science 279 (1998) 548.
[52] D. Zhao, Q. Huo, J. Feng, B.F. Chmelka, G.D. Stucky, J. Am. Chem. Soc. 120 (1998) 6024.
[53] S. Wu, Y. Han, Y.C. Zou, J.W. Song, L. Zhao, Y. Di, S.Z. Liu, F.S. Xiao, Chem. Mater. 16 (2004) 486.
[54] J. Aburto, M. Ayala, I. Bustos-Jaimes, C. Montiel, E. Terres, J.M. Dominguez, E. Torres, Microporous Mesoporous Mater. 83 (2005) 193.
[55] Y.C. Lin, C.F. Cheng, H.H. Cheng, Y.C. Chen, Chem. Phys. Lett. 164 (2004) 321.
[56] P. Rayo, M.S. Rana, J. Ramírez, J. Ancheyta, A. Aguilar-Elguézabal, Catal. Today 130 (2008) 283.
[57] G. Carja, G. Delahay, Appl. Catal. B 47 (2004) 59.
[58] X.M. Du, R.M. Almeida, J. Mater. Res. 11 (1996) 353.
[59] K. Schrijnemakers, N.R.E.N. Impens, E.F. Vansant, Langmuir 15 (1999) 5807.
[60] D.C.M. Dutoit, M. Schneider, R. Hutter, A. Baiker, J. Catal. 161 (1996) 651.
[61] Z. Luan, E.M. Maes, P.A.W. Van der Heide, D. Zhao, R.S. Czernuszewicz, L. Kevan, Chem. Mater. 11 (1999) 3680.
[62] G. Petrini, A. Cesana, G.F. De Alberti, G. Genoni, M. Leofanti, M. Padovan, G. Paparatto, P. Roffia, Stud. Surf. Sci. Catal. 68 (1991) 761.
[63] S.Y. Balaji, Raman Spectrosc. 37 (2006) 1416.
[64] A.L. Bassi, D. Cattaneo, V. Russo, C.E. Bottani, E. Barborini, T. Mazza, P. Piseri, P. Milani, F.O. Ernst, K. Wegner, S.E.J. Pratsinis, Appl. Phys. 98 (1–9) (2005) 74305.
[65] J. Konatowski, B. Wichterlova, J. Jitkovsky, E. Loffler, W. Pilz, J. Chem. Soc. Faraday Trans. 92 (1996) 1067.
[66] Q. Yang, S. Wang, J. Lu, G. Xiong, Z.C. Feng, Q. Xin, C. Li, Appl. Catal. A: Gen. 194 (2000) 507.
[67] W.H. Zhang, J. Lu, B. Han, M. Li, J. Xiu, Y.P. Ying, C. Li, Chem. Mater. 14 (2002) 3413.
[68] V.V. Atuchin, V.G. Kesler, N.V. Pervukhina, Z. Zhang, J. Electron Spectrosc. Relat. Phenom. 152 (12) (2006) 18.
[69] A. Di Giuseppe, M. Crucianelli, F. De Angelis, C. Crestini, R. Saladino, Appl. Catal. B: Environ. 89 (2009) 239–245.
[70] J. Xiao, L. Wu, Y. Wu, B. Liu, L. Dai, Z. Li, Q. Xia, H. Xi, Appl. Energy 113 (2014) 78–85.
[71] X.-M. Yan, P. Meia, J. Lei, Y. Mi, L. Xiong, L. Guo, J. Mol. Catal. A: Chem. 304 (2009) 52.
[72] J. Qiu, G. Wang, D. Zeng, Y. Tang, M. Wang, Y. Li, Fuel Process. Technol. 90 (2009) 1538.
[73] C. Komintarachat, W. Trakarnpruk, Ind. Eng. Chem. Res. 45 (2006) 1853.
[74] H. Ling, B.X. Shen, X.L. Zhou, Z.J. Gang, J. East China Univ. Sci. Technol. (Nat. Sci. Ed.) 31 (2005) 48.
[75] M.G. Clerici, Top. Catal. 13 (2000) 373.
[76] I.W.C.E. Arends, R.A. Sheldon, Appl. Catal. A: Gen. 212 (2001) 175.
[77] J.S. Rafelt, J.H. Clark, Catal. Today 57 (2000) 33.
[78] A. Corma, Chem. Rev. 97 (1997) 2373.